The solute carrier SLC35F2 enables YM155-mediated DNA damage toxicity

Georg E. Winter, Branka Radic, Cristina Mayor-Ruiz, Vincent A Blomen, Claudia Trefzer, Richard K. Kandasamy, Kilian V.M. Huber, Manuela Gridling, Doris Chen, Thorsten Klampfl, Robert Kralovics, Stefan Kubicek, Oscar Fernandez-Capetillo, Thijn R. Brummelkamp and Giulio Superti-Furga

Supplementary Results

Supplementary Figure Legends

Supplementary Figure 1

(a) Cellular viability of KBM7^{WT}, KBM7^{GT1} and KBM7^{recon} cells after 72 hours of exposure to various concentrations of nilotinib. Results represent the mean ± s.d. of triplicates. (**b)** Flag immunoblot of total cell lysates of KBM7^{WT}, KBM7^{GT1} and KBM7^{recon} that is stably reconstituted with C-terminal Flag tagged SLC35F2. Asterisk depicts unspecific band. **(c)** SLC35F2 and GAPDH mRNA levels in KBM7^{WT}, KBM7^{GT1}, KBM7^{recon}. (b) and (c) are representative of three independent experiments, see Supplementary Figure 11 for uncropped gel images.

Supplementary Figure 2

(a) Depiction of log2 transformed read counts of KBM7^{WT} or KBM7^{GT1} cells treated for six hours with either YM155 (1 μM) or vehicle (DMSO) control. (**b)** Selected genesets enriched in YM155 treated KBM7^{WT} cells indicative of a DNA damage response or induction of apoptosis.

Supplementary Figure 3

(a) Tail moment means from comet assays performed on SW480 cells exposed to ionizing radiation (IR) or YM155. Note that whereas in response to IR all cells present a comet tail, the comet assay from YM155-exposed cells shows a bimodal response with only 34,7% of the cells showing a detectable comet tail. **(b)** Example images from the comet assay explained in *a*. **(c)** EdU incorporation rates in SW480 cells exposed to YM155 or Aphidicolin analyzed by High Throughput Microscopy. **(d)** High Throughput Microscopy mediated analysis of gH2AX and DAPI levels per individual nucleus in SW480 cells exposed to Aphidicolin, the radiomimetic drug Neocarzinostatin and YM155. The intensity of DAPI enables to evaluate the cell cycle stage based on DNA quantity. Whereas Neocarzinostatin triggers H2AX phosphorylation on every cell regardless of the cell cycle, the profile of YM155-induced gH2AX is equivalent to the one induced by Aphidicolin, with the response being restricted to replicating cells. Noteworthy, a 1 hour pre-treatment with aphidicolin followed by 3 hours of YM155 gives a similar profile as

cells exposed to either drug alone. The doses uses for all panels were: YM155 (100 nM, 3 h), Aphidicolin (APH; 5 mM, 3 h), IR (20Gy) and Neocarzinostatin (50 ng/ml, 3 h). Note: SW480 cells rather than KBM7 were used for this Figure to facilitate the High Throughput Microscopy analyses shown in *c* and *d* due to these cells being adherent. (a)-(d) are representative of three independent experiments.

Supplementary Figure 4

FACS plots of $KBM7^{WT}$, $KBM7^{GT1}$ and $KBM7^{recon}$ cells after 16 hours of exposure to various concentrations of YM155 depicting PI and annexin V signal intensities. Representatives of three independent experiments.

Supplementary Figure 5

Intracellular YM155 levels depicted as arbitrary units determined with MRM in HEK293T cells stably overexpressing C-V5 tagged SLC35F2 or empty vector control. Results represent the mean ± s.d. of triplicates

Supplementary Figure 6

(a) Schematic depiction of SLC35F2 genomic locus indicating the site that has been targeted with CRISPR based genome editing. **(b)** Representative chromatogram of Sanger sequencing reaction of subcloned PCR amplicon flanking the putative CRISPR targeting site in exon 7 in either $SW480^{WT}$ ($SLC35F2^{WT}$) cells or in the clone $SW480SLC^{mut2}$.

Supplementary Figure 7

Log2 depiction of SLC35F2 upregulation in cancer vs. normal for various malignancies as reported in Oncomine® meta-database. Values are depicted as a function of their p-value for that expression difference.

Supplementary Figure 8

EC_{50} values for **(a)** YM155, **(b)** idarubicin and **(c)** topotecan were derived for all cell lines indicated and are depicted as a function of SLC35F2 expression levels in the respective cell lines. Dose response curves were determined in triplicates and are depicted as hierarchically clustered, row-normalized (Pearson's correlation) heatmaps.

Supplementary Figure 9

Rank ordering of all genes quantified elsewhere[22] based on their Pearson's correlation with YM155 efficacy (measured by EC_{50} values) over the cell lines outlined in Figure 4B.

Supplementary Figure 10

(a) Representative images of the xenograft tumors from the different groups at the end of the experiment **(b)** Immunohistochemistry (IHC) of gH2AX (**b**) or an activated form of caspase 3 (C3A) (**c**) on xenografts 5 d after implantation of the infusion pumps. Scale bar (black) indicates 100 mm. (b) and (c) are representative of three different sections examined.

Supplementary Figure 11

Full size representation of cropped gel images shown in the indicated figures

Supplementary Figure 1

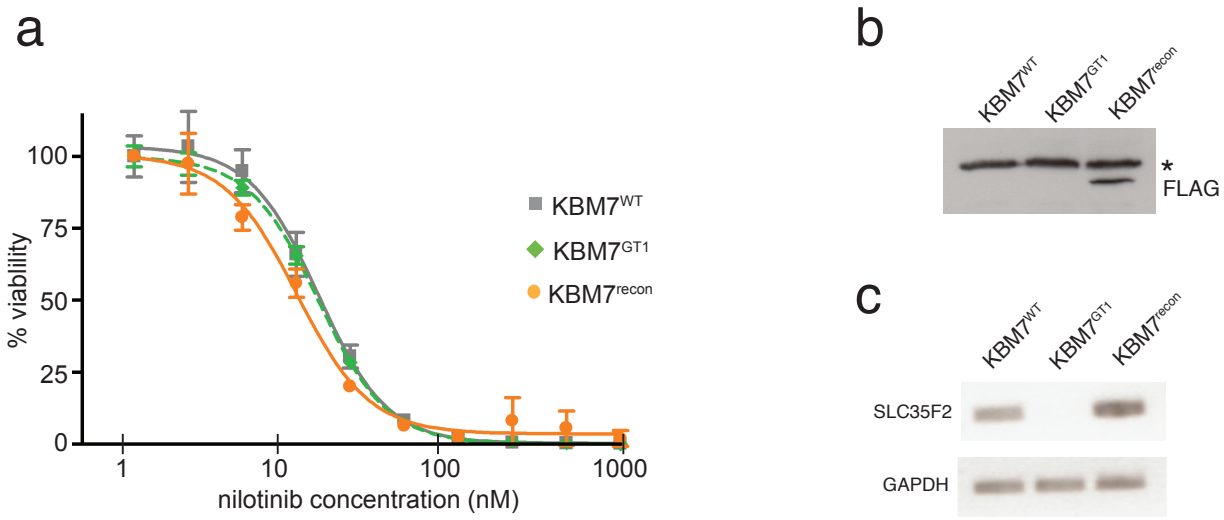

Supplementary Figure 2

a

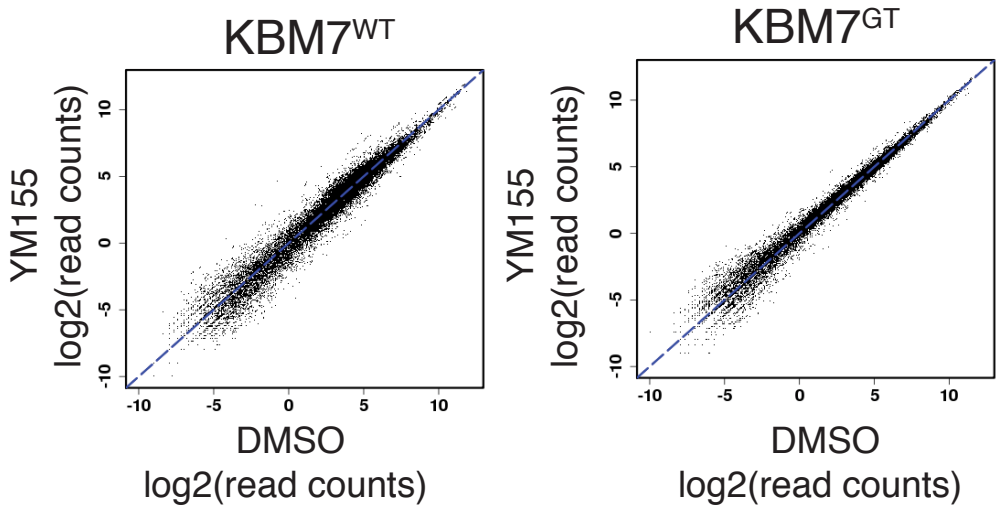

b

Significantly (p<0.001) enriched genesets (selected) Gene Set Name	# Genes in Gene Set (K)	Description	# Genes in Overlap (k)	k/K	p-value	FDR q-value
GRAESSMANN_APOPTOSIS_BY_DOXORUBICIN_DN	1781	Genes down-regulated in ME-A cells (breast cancer) undergoing apoptosis in response to doxorubicin	66	0	0.00E+00	0.00E+00
PUJANA_ATM_PCC_NETWORK	1442	Genes constituting the ATM-PCC network of transcripts whose expression positively correlated (Pearson correlation coefficient, PCC >= 0.4) with that of ATM [GeneID=472] across a compendium of normal tissues.	57	0	0.00E+00	0.00E+00
ENK_UV_RESPONSE_KERATINOCYTE_UP	530	Genes up-regulated in NHEK cells (normal epidermal keratinocytes) after UVB irradiation.	32	0	0.00E+00	0.00E+00
REACTOME_APOPTOSIS	148	Genes involved in Apoptosis	11	0	2.42E-08	1.63E-06
REACTOME_INTRINSIC_PATHWAY_FOR_APOPTOSIS	30	Genes involved in Intrinsic Pathway for Apoptosis	6	0	1.02E-07	5.71E-06
KEGG_P53_SIGNALING_PATHWAY	69	p53 signaling pathway	7	0	1.09E-06	2.53E-05
BIOCARTA_ATM_PATHWAY	20	ATM Signaling Pathway	3	0	4.69E-04	3.39E-03
REACTOME_APOPTOTIC_EXECUTION_PHASE	54	Genes involved in Apoptotic execution phase	4	0	8.08E-04	7.67E-03
BIOCARTA_DNAFRAGMENT_PATHWAY	10	Apoptotic DNA fragmentation and tissue homeostasis	2	0	2.56E-03	1.42E-02
BIOCARTA_P53_PATHWAY	16	p53 Signaling Pathway	2	0	6.61E-03	2.76E-02
BIOCARTA_CHEMICAL_PATHWAY	22	Apoptotic Signaling in Response to DNA Damage	2	0	1.23E-02	4.32E-02

Supplementary Figure 3

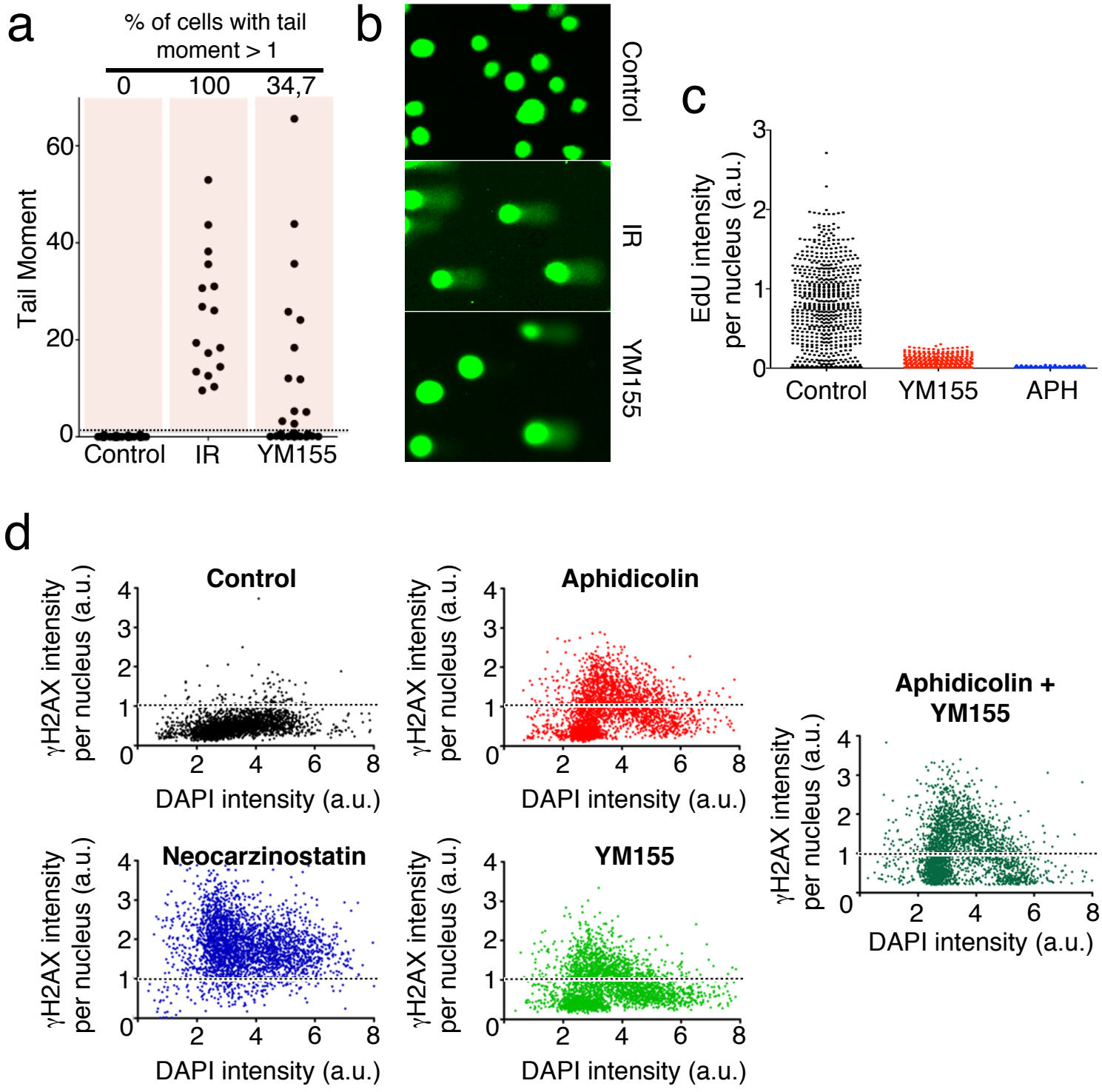

Supplementary Figure 4

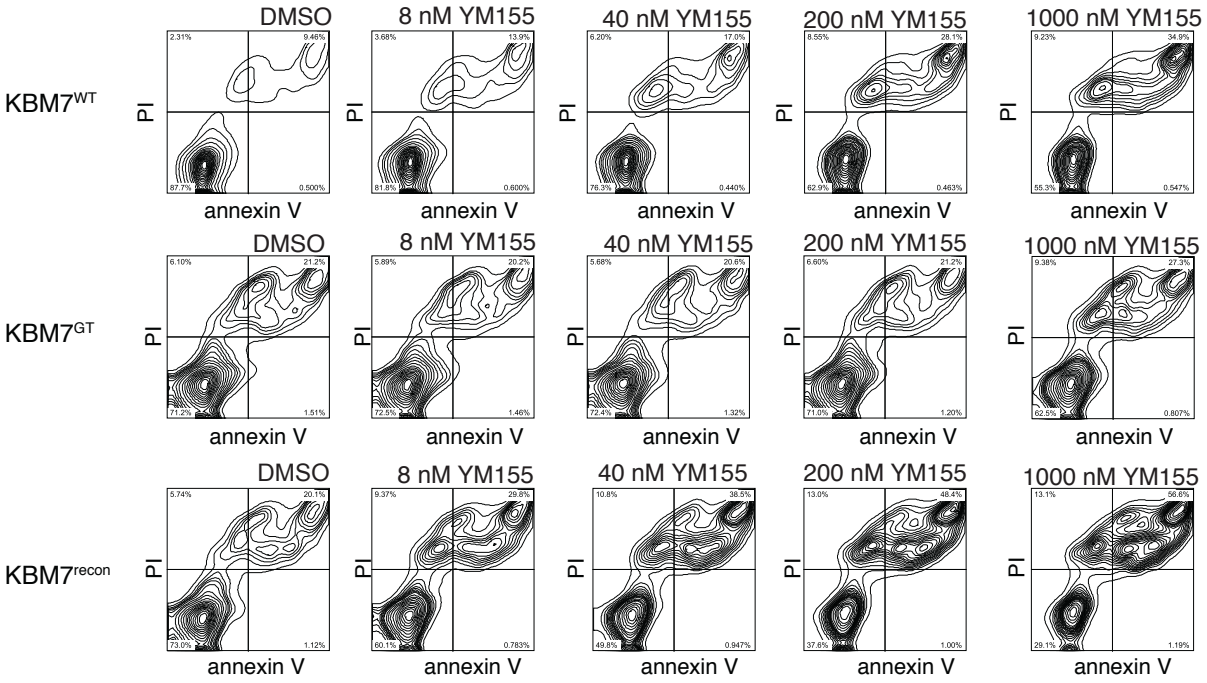

Supplementary Figure 5

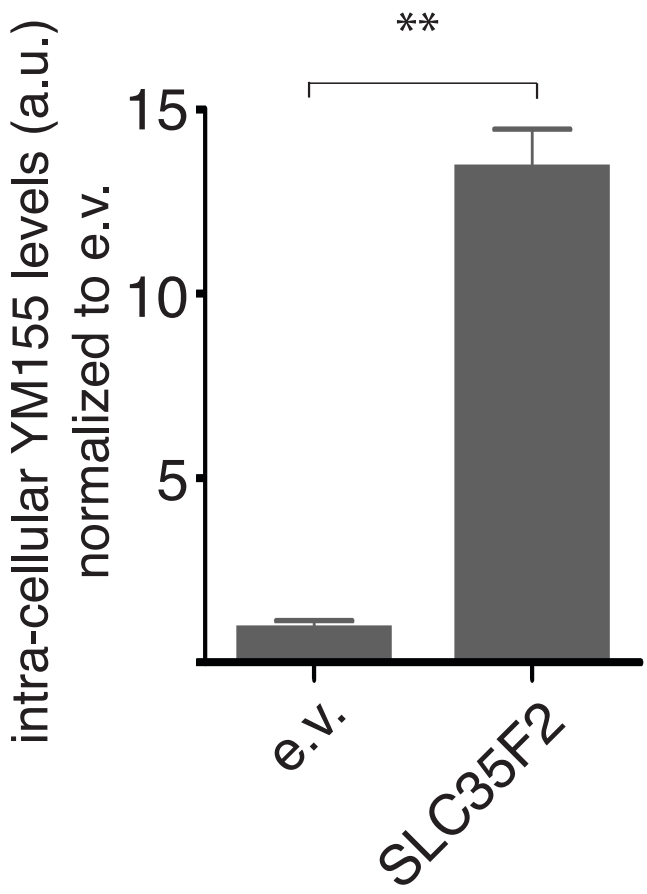

Supplementary Figure 6

Supplementary Figure 7

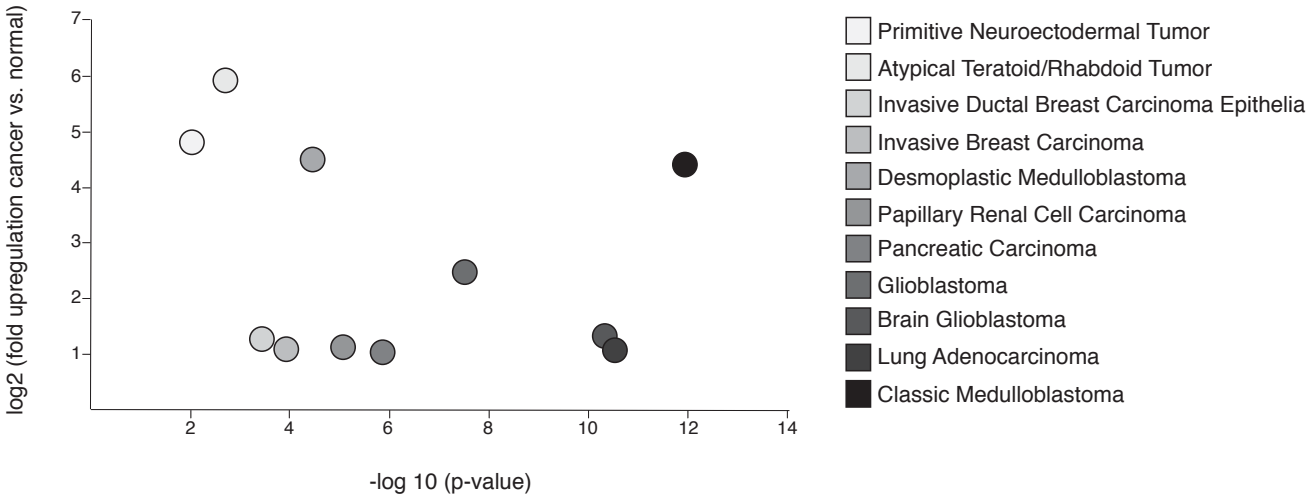

Supplementary Figure 8

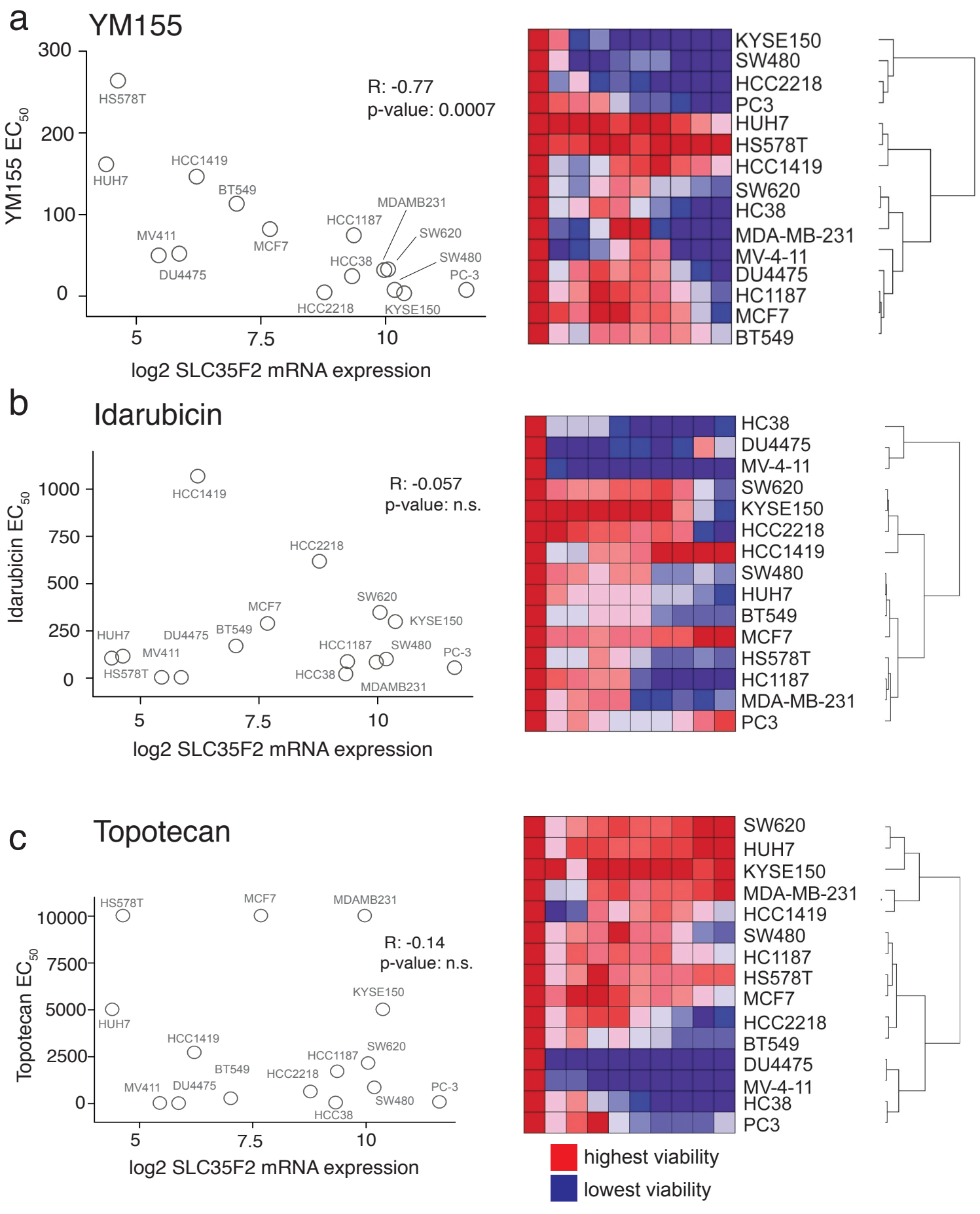

Supplementary Figure 9

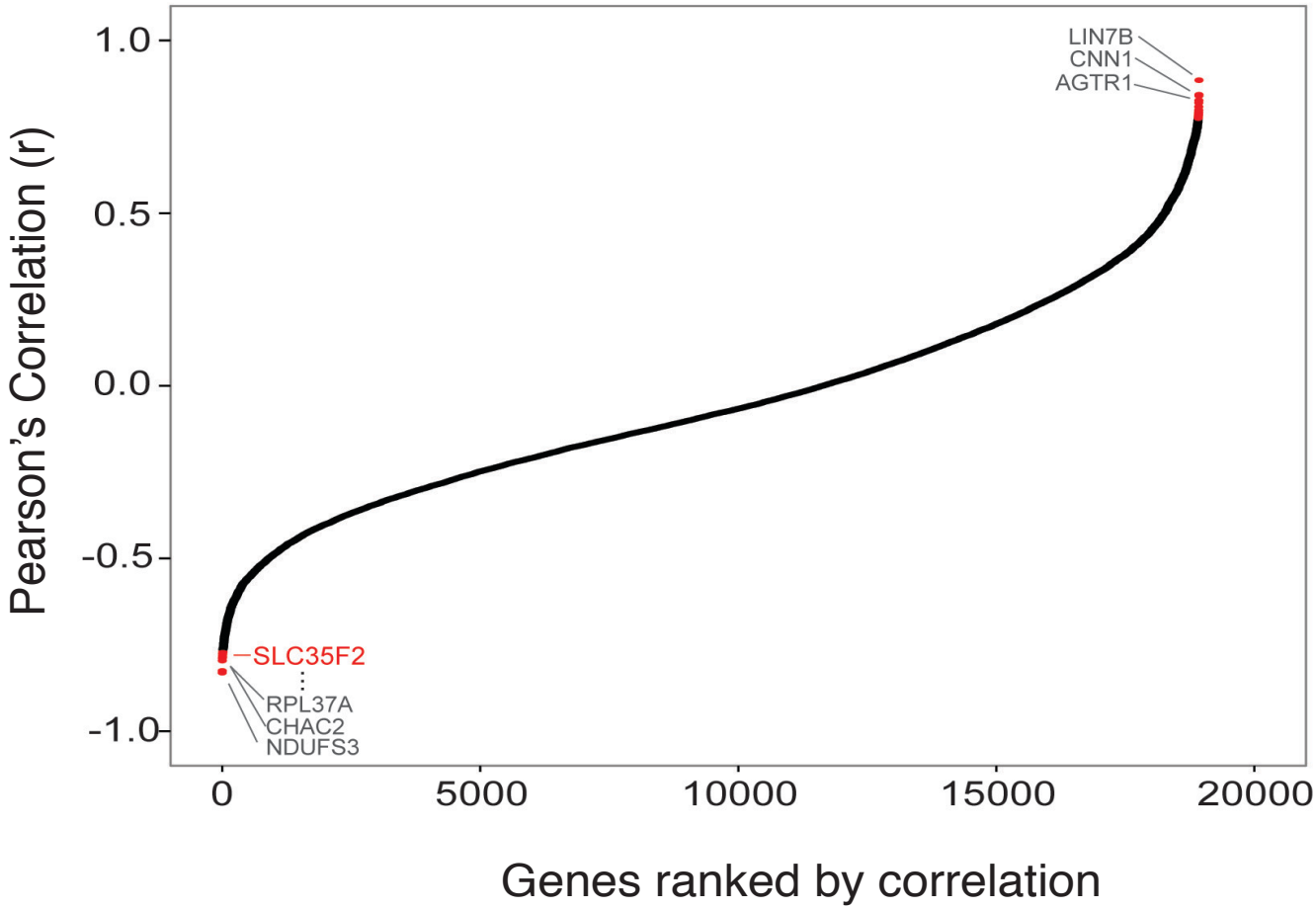

Supplementary Figure 10

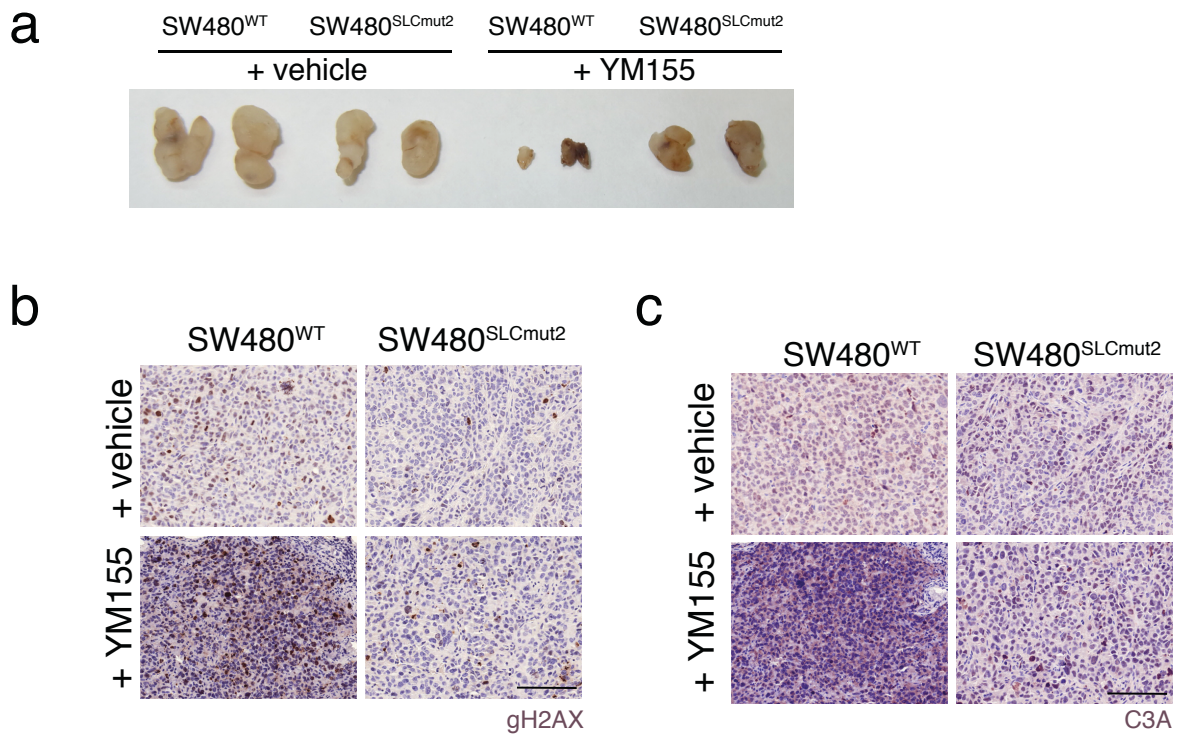

Supplementary Figure 11

Fig 1d

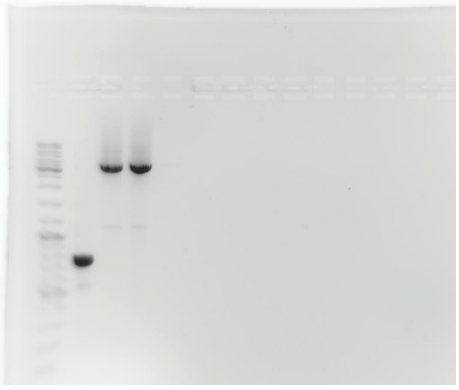

Fig 1e

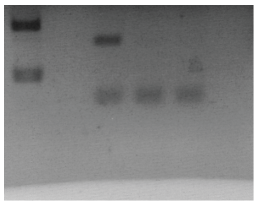

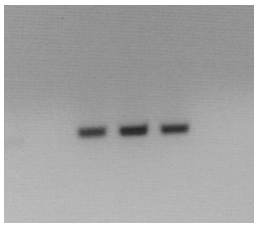

Fig 2c

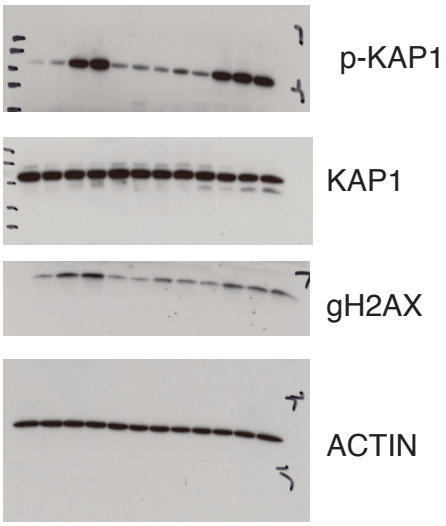

Fig 2d

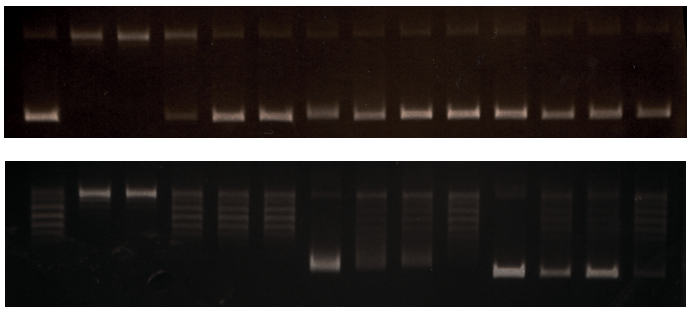

Fig 4d

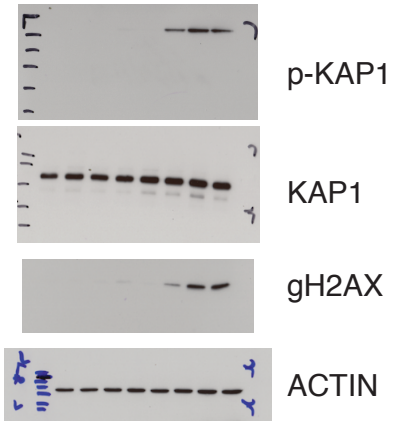

Suppl Fig 1b

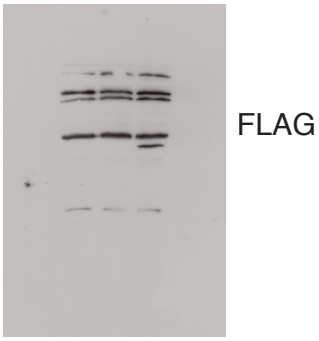

Suppl Fig 1c
SLC35F2

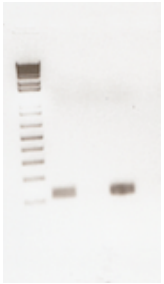

Suppl Fig 1c
GAPDH